BRIEF DEFINITIVE REPORT

# Molecular imaging of Alzheimer's disease–related gamma-secretase in mice and nonhuman primates

Yulong Xu[1], Changning Wang[1], Hsiao-Ying Wey[1], Yingxia Liang[2], Zude Chen[1], Se Hoon Choi[2], Chongzhao Ran[1], Kevin D. Rynearson[3], Daniela R. Bernales[1], Robert E. Koegel[1], Stephanie A. Fiedler[1], Robin Striar[1], Steven L. Wagner[3,4], Rudolph E. Tanzi[2], and Can Zhang[2]

The pathogenesis of Alzheimer's disease (AD) is primarily driven by brain accumulation of the amyloid-β-42 ($A\beta_{42}$) peptide generated from the amyloid-β precursor protein (APP) via cleavages by β- and γ-secretase. γ-Secretase is a prime drug target for AD; however, its brain regional expression and distribution remain largely unknown. Here, we are aimed at developing molecular imaging tools for visualizing γ-secretase. We used our recently developed γ-secretase modulators (GSMs) and synthesized our GSM-based imaging agent, [$^{11}$C]SGSM-15606. We subsequently performed molecular imaging in rodents, including AD transgenic animals, and macaques, which revealed that our probe displayed good brain uptake and selectivity, stable metabolism, and appropriate kinetics and distribution for imaging γ-secretase in the brain. Interestingly, rodents and macaques shared certain brain areas with high γ-secretase expression, suggesting a functional conservation of γ-secretase. Collectively, we have provided the first molecular brain imaging of γ-secretase, which may not only accelerate our drug discovery for AD but also advance our understanding of AD.

## Introduction

Alzheimer's disease (AD) is a neurodegenerative disorder and the primary cause of dementia. Currently, there are no approved therapeutics that completely stop or reverse the cognitive deficits associated with AD. With increasing life expectancy and an aging baby boomer generation, the prevalence of this age-related disease is predicted to increase by more than 40% in 10 yr. The current standard of care only slows or delays the progression of this insidious disease, potentially intensifying the social and economic costs of the disease.

The molecular neuropathology of AD is characterized by two hallmarks: β-amyloid plaques primarily composed of a small protein, amyloid-β (Aβ; Bertram and Tanzi, 2008; Choi et al., 2014; Cummings, 2004; Hardy and Selkoe, 2002); and neurofibrillary tangles (NFTs) composed of hyperphosphorylated tau protein. Although the underlying mechanisms of AD have not been completely elucidated, considerable evidence supports the "Aβ hypothesis," positing that excessive accumulation of Aβ is the primary pathological event of AD, which induces the formation of NFTs, followed by neuroinflammation and neurodegeneration in AD (Bertram and Tanzi, 2008; Choi et al., 2014; Gandy, 2005; Hardy and Selkoe, 2002; Park et al., 2018). Aβ is

produced via a serial cleavage of the Aβ precursor protein (APP) by β- and γ-secretase. While $A\beta_{42}$ and $A\beta_{40}$ are the two primary Aβ species, $A\beta_{42}$ is more aggregation prone and more prevalent than $A\beta_{40}$ in β-amyloid plaques in the brain (Bertram and Tanzi, 2008; Choi et al., 2014; Hardy and Selkoe, 2002). Thus, an effective therapeutic for AD should preferentially decrease $A\beta_{42}$ levels (Choi et al., 2014; Zhang, 2017).

Particularly, γ-secretase cleavage of APP, following β-processing of APP, determines the length of Aβ species and can be modulated to decrease $A\beta_{42}$ levels. Thus, selectively modulating γ-secretase activity has emerged as a potential disease therapeutic strategy for AD, because γ-secretase modulators (GSMs) can reduce the formation of pathogenic $A\beta_{42}$ species while displaying little or no effects on non-APP substrates of γ-secretase, such as Notch (Brendel et al., 2015; Imbimbo et al., 2007; Kounnas et al., 2010; Rogers et al., 2012). Several GSMs have been reported and can be largely divided into two categories, including the early-stage nonsteroidal anti-inflammatory drug (NSAID)–derived carboxylic acid–containing GSMs and non-NSAID imidazole–containing GSMs. For example, CHF5074 is a NSAID-like compound that displays $IC_{50}$ (inhibitory

concentration of reduction by 50%) of decreasing $A\beta_{42}$ of 3.6 μM in cell-based studies with promising results in AD mouse model–based studies (Imbimbo et al., 2007; Sivilia et al., 2013) and safety profiles in human trials (Imbimbo et al., 2013). The other two compounds, RO5506284 (Brendel et al., 2015) and EVP-0015962 (Rogers et al., 2012), both displayed over 20 nM in $IC_{50}s$ of $A\beta_{42}$ from cell-based studies and reduced β-amyloid pathology, one also displayed improved behavioral deficits in AD mouse mice (Rogers et al., 2012).

## Results and discussion

We have developed a series of new GSMs that display high potential in AD therapeutics. We first described aryl 2-aminothiazole class parent GSMs (Kounnas et al., 2010) with relatively low aqueous solubility (Fig. S1) and then developed aryl 2-aminothiazole class soluble GSMs (SGSMs) with increased aqueous solubility but relatively lower $IC_{50}$ in reducing $A\beta_{42}$ (Raven et al., 2017; Wagner et al., 2014; SGSM-36; Fig. S1). We recently developed a novel series of pyridazine class SGSMs and reported SGSM-15606 with excellent solubility, potency in reducing $A\beta_{42}$ levels, and desirable drug-like properties (Wagner et al., 2017; Fig. S1 and Table S1). Moreover, our GSMs were characterized with mechanism of actions in targeting $A\beta_{42}$ related to binding γ-secretase components, particularly PS1 fragments using cell-based affinity chromatography analysis (Kounnas et al., 2010). Additionally, our GSMs may access and act on an allosteric site within PS1, which leads to a conformational change in PS1 (Raven et al., 2017). Our findings further supported the results of other studies showing that pharmacological agents targeting γ-secretase bind the PS1–γ-secretase complex and induce conformational changes within the active sites of γ-secretase (Gertsik et al., 2015; Pozdnyakov et al., 2013). GSM gaining access to PS1 may be related to γ-processing of APP, resulting in changes in the levels and isoforms of Aβ species (Raven et al., 2017). Collectively, these mechanism-based studies on the molecular level and pharmacological studies strongly support our SGSMs, particularly SGSM-15606, in clinical development for AD intervention.

In this study, we set out to investigate whether our SGSMs may be used in molecular imaging for PS1 proteins and investigation of AD (Table S1). Particularly, noninvasive molecular imaging methods, such as positron emission tomography (PET), have been developed to visualize and analyze the biochemistry-based molecular targets in inaccessible tissues (e.g., the brain) and therefore provided distinct advantages for AD-related studies. The methods are different from in vitro techniques that cannot provide analyses of systems-level intact organisms over time in endogenous environment. Specifically, in vivo molecular PET imaging of AD has been developed as an important tool to evaluate AD pathological progresses and stages. Moreover, the PET ligands, including those for Aβ plaques (Klunk et al., 2004; Landau et al., 2014; Nordberg, 2004) and neurofibrillary tau tangles (Choe and Lee, 2015; James et al., 2015; Okamura et al., 2014), are widely used and becoming more routine in clinical trials and neuropathology evaluation. Earlier this year, a report described the development of β-secretase, or BACE1, PET ligands in nonhuman primates

(NHPs; Zhang et al., 2018). Several PS1 tritium radiotracers have been developed based on inhibitory or modulatory mechanisms of γ-secretase in vitro (Iben et al., 2007; Liu et al., 2013; Patel et al., 2006; Yan et al., 2004). However, there are no reports on PET imaging probe targeting γ-secretase in animals and humans, to our knowledge. Thus, the goal of our project is to enhance our GSM development program through investigating the SGSM brain engagement in vivo by developing the first PET radiotracer targeting γ-secretase in animal brains.

Development of specific PET radiotracers to measure γ-secretase density or any other central nervous system component with high uptake is challenging (Wang et al., 2014). A number of major factors have been identified that determine the success of a radiotracer candidate. We have focused on these factors in our current studies, which were described below.

### Synthesis of [11C]SGSM-15606 that readily enter the brains

Certain criteria determines the ability of a potential PET tracer to penetrate the blood–brain barrier (BBB) and become a valid imaging tool. We therefore evaluated a recently reported lead compound from our the new pyridazine class, SGSM-15606, in crossing the BBB. Usually, properties including small molecular weight (<500 daltons) and a high degree of lipophilicity may favor a tracer to pass the lipid bilayer of the BBB. Furthermore, predictive models based on PET imaging data suggest values of the total polar surface area (tPSA) of <76 (Seo et al., 2014). The molecular weight and tPSA of SGSM-15606 are within the typical range for small molecules that demonstrate good brain penetration (Table S1). We radiolabeled SGSM-15606 at the hydroxyl position with $[^{11}C]CH_3I$ to lead to $[^{11}C]SGSM-15606$ (Fig. 1 A). It was prepared in 30–35 min after the end of bombardment, with radiochemical yields (2–8%, uncorrected for decay and based on trapped $[^{11}C]CH_3I$), high radiochemical purity, and high chemical purity (>97%).

Next, we performed self-blocking study to further characterize the binding affinity and selectivity of our $[^{11}C]SGSM-15606$ in rodents. Particularly, wild-type C57BL/6 mice (25–30 g, male, 15 wk old) were treated with or without SGSM-15606 5 min before injection of $[^{11}C]SGSM-15606$ (Fig. 1, B–E). We showed that brain uptake of $[^{11}C]SGSM-15606$ was ~50% reduction based on AUC (area under curve) compared with baseline uptake (Fig. 1 E). The highest brain uptake was observed at 3 min. The behavior of $[^{11}C]SGSM-15606$ in the blocking scans showed an injection peak followed by faster washout over time, while the slower washout was observed in the baseline scans. A more steady TAC in the baseline scans resulted in higher activity levels at the end of the scan. These results of the blocking study revealed that $[^{11}C]SGSM-15606$ showed high brain uptake and good specific binding by our self-blocking analysis. Thus, our results indicate that $[^{11}C]SGSM-15606$ would serve as a imaging tool for new GSM target engagement measurement and accelerate the GSM development as potential AD therapeutics.

The binding affinity and selectivity of a radiotracer for its target must be high enough to produce sufficient signal for detection. Here, SGSM-15606 displayed excellent biological ability in both specificity and potency ($IC_{50}$ of $A\beta_{42}$ = 7 nM). Unlike γ-secretase inhibitors (Kreft et al., 2009), which inhibit the
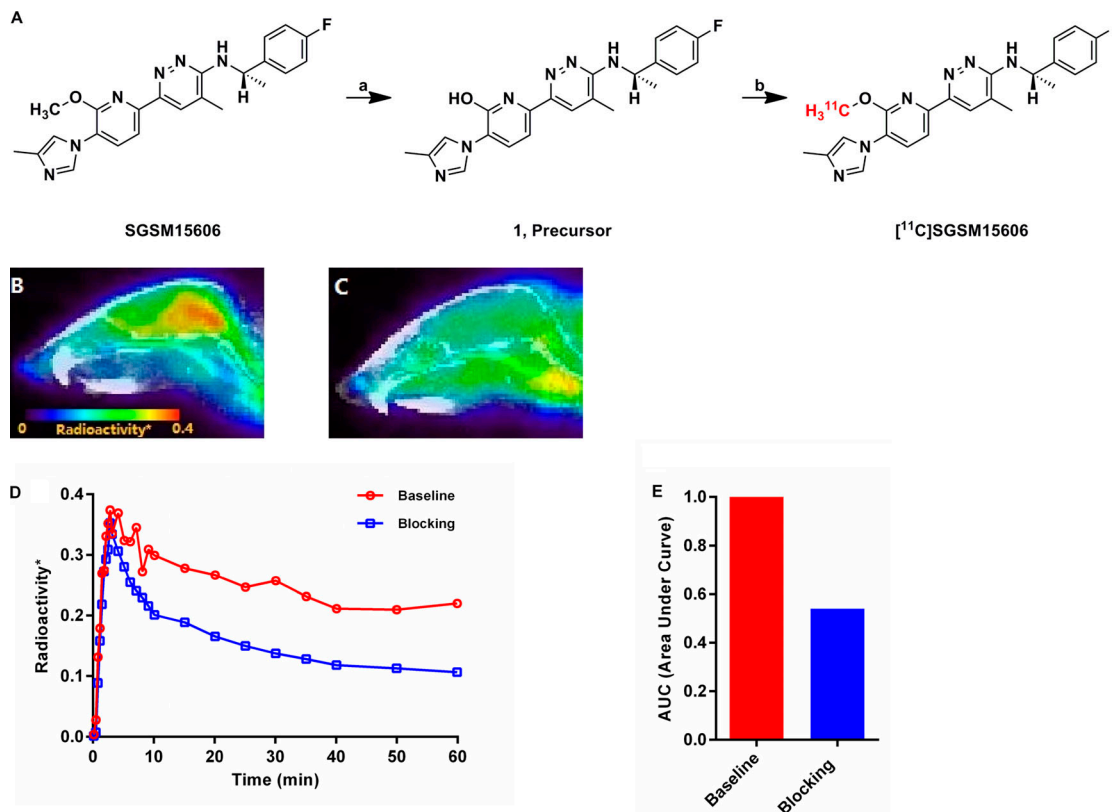
Xu et al.
Visualizing Alzheimer's gamma-secretase

Journal of Experimental Medicine    2 of 9
https://doi.org/10.1084/jem.20182266

Figure 1. **Radiosynthesis of [¹¹C]SGSM-15606 and PET-CT–blocking analysis. (A)** Reaction conditions: (a) TMS-Cl, NaI, MeOH, reflux, 2 h, >80%; (b) 1 (precursor, 0.5 mg), [¹¹C]CH3I, CsCO3 (5 mg), in 300 µl DMSO, 3 min, 50°C. Radiochemical yield: 2–5% (nondecay corrected to trapped [¹¹C]CH3I). **(B and C)** PET-CT blocking analysis of [¹¹C]SGSM-15606 in C57BL/6 wild-type mice (male, 15 wk old). PET-CT image of [¹¹C]SGSM-15606 at baseline (B; $n = 2$) or following pretreatment with 1.0 mg/kg of SGSM-15606 (C; $n = 2$). Mice were from The Jackson Laboratory. **(D)** TACs of whole-brain uptake of [¹¹C]SGSM-15606 of B and C. *, whole-brain radioactivity normalized by maximal blood radioactivity. **(E)** AUC for TACs of baseline and blocking (30–60 min, ∼50% reduction in AUC).

production of all Aβ peptides, GSMs bind PS1 components and do not affect the total amount of Aβ produced. Also, GSMs do not result in an accumulation of APP-CTFs or affect processing of other γ-secretase substrates, including Notch. Based on the MDR1-MDCK assay, SGSM-15606 is not a P-glycoprotein substrate, and no significant off-target binding with Centre d'Enseignement et de Recherche en Etudes Postcoloniales profiling, with reported pharmacological and toxicological properties (Table S1; Wagner et al., 2017).

### PET imaging for PS1/γ-secretase in brains of AD transgenic mice

After we synthesized and validated our [¹¹C]SGSM-15606, we further used our new tracer to evaluate the expression and distribution of PS1/γ-secretase in AD. Particularly, we used the previously reported 5XFAD transgenic mice that express APP[Swedish/Florida/London] PS1[M146L/L286V] (Oakley et al., 2006; Youmans et al., 2012) compared with wild-type animals. 10-wk-old female transgenic or wild-type control mice were subjected to PET imaging analysis using [¹¹C]SGSM-15606. Our results revealed steady and robust up-regulation of brain radioactivity of [¹¹C]SGSM-15606 in brains of AD transgenic mice (Figs. 2, A–C). Additionally, we performed quantification analysis showing the time–activity curves (TACs) of whole-brain uptake of [¹¹C]SGSM-15606 comparing AD to mice, represented by the percentage of injected dose per cubic centimeter. Our results

showed that the brain uptake of [¹¹C]SGSM-15606 in transgenic animals was related to a 2.3-fold increase in brain uptake compared with that of the control mice, and also reached a percentage of injected dose per cubic centimeter plateau of ∼3.5 at the end of the scan (Fig. 2 C). Furthermore, we performed brain regional analysis for PS1/γ-secretase expressions after i.v. injection of [¹¹C]SGSM-15606 and sagittal superimposition of corresponding template magnetic resonance imaging (MRI; Fig. 3, A–D). We found that [¹¹C]SGSM-15606 revealed higher uptake in several brain regions, including cortex, hippocampus, and midbrain comparing transgenic to wild-type animals (Fig. 3, A–D). Our results on brain imaging revealed brain regional and differential expression of PS1/γ-secretase. Because γ-secretase plays critical roles in AD, our findings provided new insights of γ-secretase in AD and may also complement the knowledge of γ-secretase concerning cellular and structural biology (Bai et al., 2015; Chávez-Gutiérrez et al., 2012; Liu et al., 2019). Collectively, our findings suggest that [¹¹C]SGSM-15606 has provided a valid imaging tool to further study AD, potentially in humans.

### NHP PET/MRI study and metabolic stability analysis

So far, our data suggested that our new [¹¹C]SGSM-15606 tracer may be potentially used in AD patients to evaluate brain PS1/γ-secretase. Therefore, we performed an NHP experiment to evaluate the translational potential of our [¹¹C]SGSM-15606
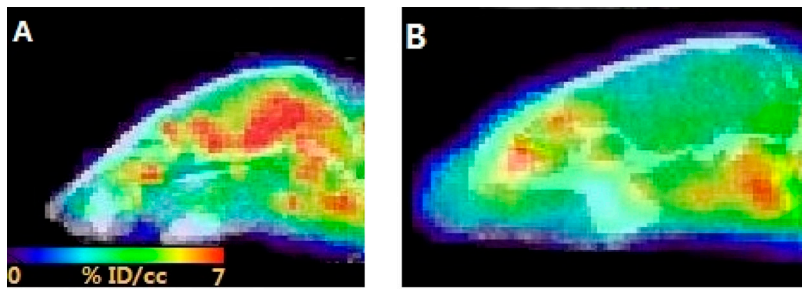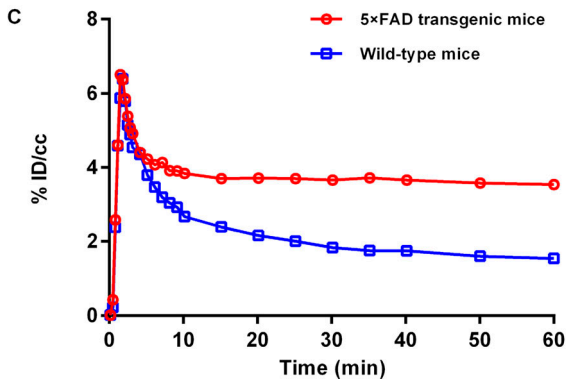
Figure 2. **PET-CT analysis of PS1/γ-secretase in 5XFAD transgenic and wild-type mice**. **(A)** PET-CT image of 5XFAD transgenic mice ($n$ = 2) after i.v. injection of [$^{11}$C] SGSM-15606. **(B)** PET-CT image of wild-type mice ($n$ = 2) after i.v. injection of [$^{11}$C]SGSM-15606. **(C)** TACs of whole brain uptake of [$^{11}$C]SGSM-15606 in A and B. Data are expressed as the percentage of injected dose per cubic centimeter (% ID/cc). B6SJL 5XFAD transgenic and wild-type mice (B and C) were from The Jackson Laboratory.

tracer as a possible step forward toward human studies. Our results demonstrated high brain uptake (0.8–3.0 in standardized uptake value [SUV]) of [$^{11}$C]SGSM-15606 based on PET-MRI (Fig. 4 A). Notably, relatively higher uptake was observed in regions such as midbrain and anterior cingulate cortex (Fig. 4, B and C). Rodents and macaques shared certain brain areas, particularly midbrain, that highly express γ-secretase, suggesting a functional conservation of γ-secretase.
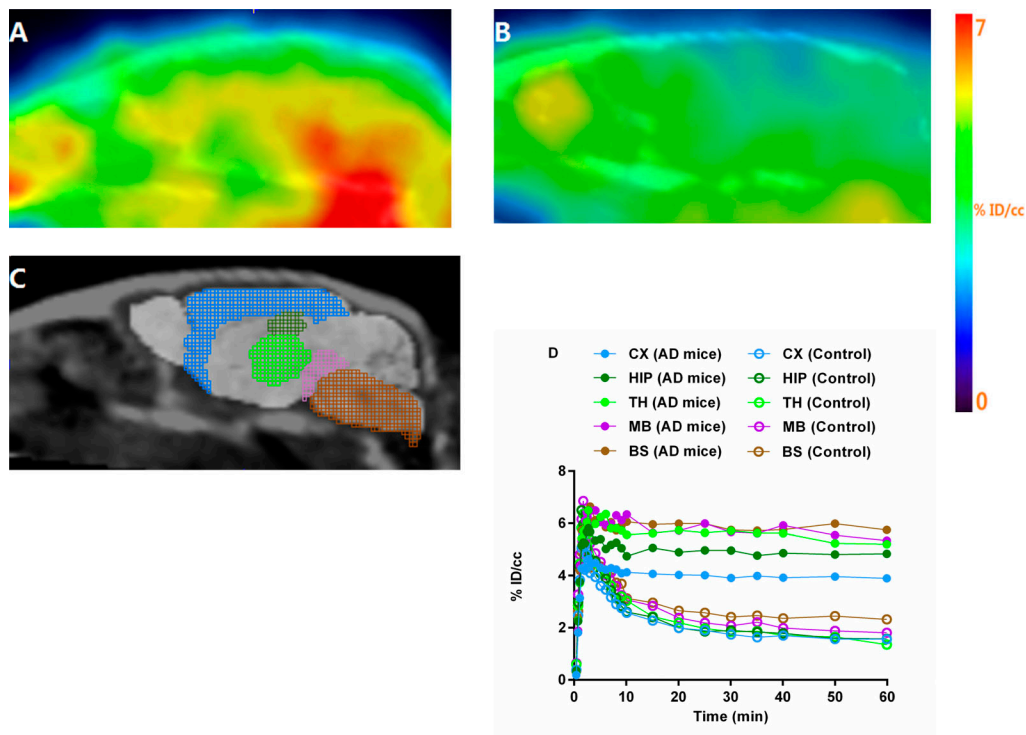


Figure 3. **Brain regional PS1/γ-secretase expression in 5XFAD transgenic and wild-type mice**. **(A)** Representative PET images of 5XFAD transgenic mice ($n$ = 2) after i.v. injection of [$^{11}$C]SGSM-15606. **(B)** Representative PET images of wild-type mice ($n$ = 2) after i.v. injection of [$^{11}$C]SGSM-15606. **(C)** Sagittal sections were superimposed on the corresponding template MRI. **(D)** TACs for brain regions of A and B. BS, brainstem; CX, cortex; HIP, hippocampus; MB, midbrain; TH, thalamus. Data were expressed as the percentage of injected dose per cubic centimeter (% ID/cc). B6SJL 5XFAD transgenic and wild-type mice (A–D) were from The Jackson Laboratory.
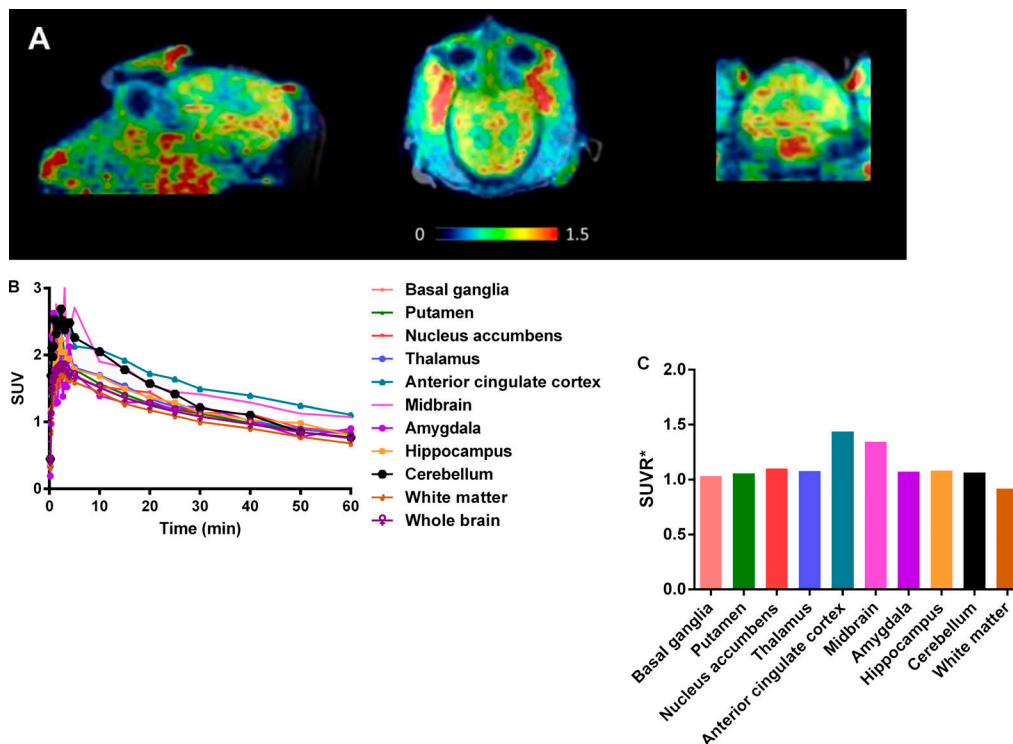
Figure 4. **PET-MRI imaging of PS1/γ-secretase in macaque brain. (A)** Summed PET images (0–60 min) superimposed with MEMPRAGE-MRI of macaque brains following injection of [11C]SGSM-15606. **(B)** Time-dependent (0–60 min) activity curves for brain regions of interest. **(C)** SUV ratio (SUVR; 30–60 min) of brain regions of interest. *, SUV of brain regions of interest normalized by SUV of whole brain.

Furthermore, we performed kinetic modeling to estimate the volume of distribution ($V_T$) values, because kinetic modeling analysis with an arterial plasma input function are considered the gold standard for quantitation of target enzyme expression. We used a two-tissue compartment (2-TC) model to analyze dynamic [11C]SGSM-15606 PET data in the NHP brain. Our kinetic modeling results showed different expression levels of [11C]SGSM-15606 across brain regions (Fig. 5 A). [11C]SGSM-15606 was expressed across different brain regions, and the levels in midbrain and anterior cingulate cortex displayed high levels (Fig. 5 A). A tracer candidate can still be rendered unusable in vivo if it is metabolized rapidly and those metabolites pervade regions of interest. In addition, knowledge of SGSM-15606 metabolism is important for modeling its distribution kinetics and assessing safety profiles (Table S1). The appearance of labeled metabolites in arterial plasma after [11C]SGSM-15606 i.v. injection was depicted (Fig. 5 B). After 10 min, <10% of the total radioactivity in arterial plasma corresponded to [11C]SGSM-15606, indicating fast washout of the radiotracer from blood. The stability evaluated in plasma over time showed lasting presence of >70% of parent compound at 30 min (Fig. 5 C). Collectively, our results suggested that PET neuroimaging by [11C]SGSM-15606 allowed us to visualize γ-secretase in brain regions in preclinical animals, which highly support great potentials for clinical studies in AD patients.

Our GSM-based probe has provided a potential useful tool that can be applied in combination with other probes/drugs or approaches to better define the pathology of AD. For example, [18F] PF-06684511 has been recently developed as a PET imaging probe for BACE1 (Zhang et al., 2018). Based on the NHP imaging with [18F] PF-06684511, BACE1 has a higher expression in AD-related brain regions such as cortex and hippocampus, which shows similar distribution with our NHP study using [11C]SGSM-15606. With these PET probes imaging secretases responsible for Aβ generation, we could study the function/expression of the APP cleavage enzymes noninvasively in the brain. More importantly, in combination with other established AD PET probes, such as the probes for amyloid plaque and tau PET imaging, we can have deeper understanding of AD etiology and accelerate therapeutic development for curing AD.

In summary, [11C]SGSM-15606 is a radiolabeled GSM with high selectivity and high brain uptake and provide a tool for quantitative imaging for PS1/γ-secretase in the brain in vivo. [11C]SGSM-15606 can be used as a γ-secretase–based PET radioligand to investigate not only the roles of γ-secretase in AD pathogenesis but also γ-secretase–based therapeutics in AD intervention. At present, the safety and toxicology studies of SGSM-15606 have been completed, and we have developed the first γ-secretase PET radiotracer in animals. In future studies, it is important that we characterize and optimize [11C]SGSM-15606 for further evaluation as a potential PET radiotracer in humans.

## Materials and methods
### General methods and materials
All reagents and solvents were of American Chemical Society–grade purity or higher and used without further purification. SGSM-15606 has been previously reported (Wagner et al., 2017).
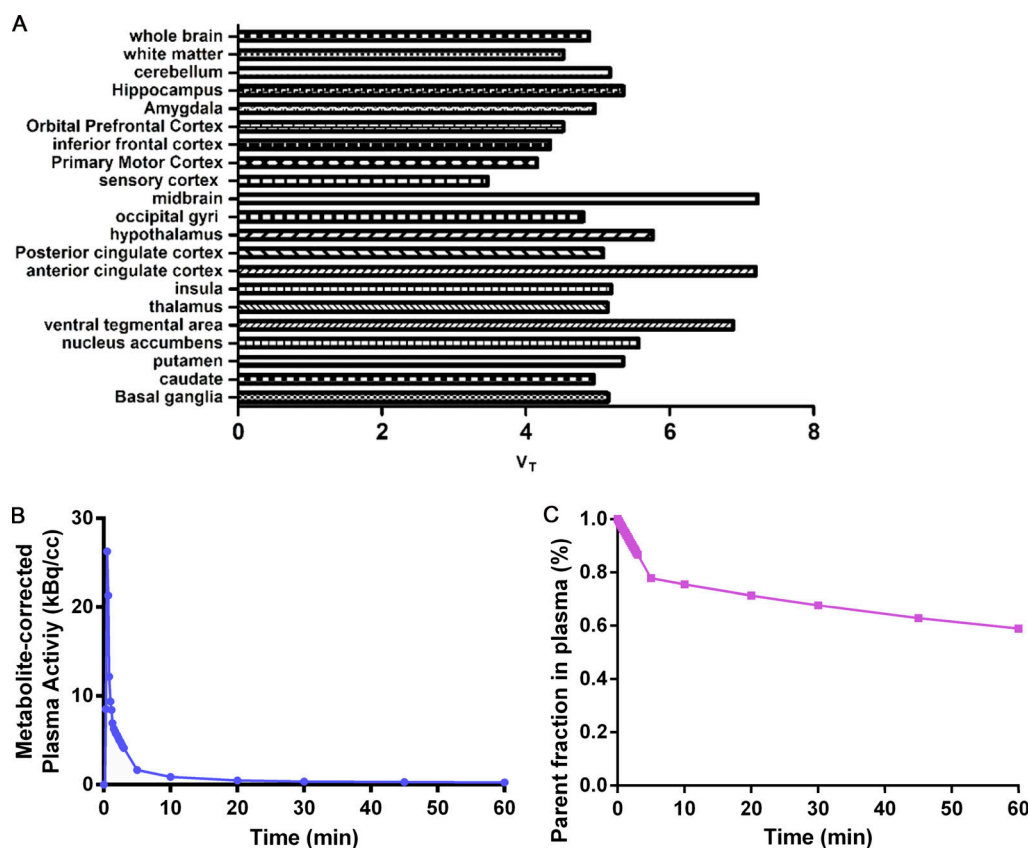
**Figure 5.** **Kinetic modeling of [11C]SGSM-15606 in macaque brain and plasma analysis. (A)** Kinetic modeling of [¹¹C]SGSM-15606 in macaque brain. $V_T$ data of 2-TC kinetic modeling showed PS1/γ-secretase in different brain regions. The top two areas included the midbrain and the anterior cingulate cortex. **(B)** Plasma radioactivity analysis of [¹¹C]SGSM-15606. Arterial plasma analysis revealed that the radioactivity was rapidly cleared from blood. **(C)** Plasma stability analysis of [¹¹C]SGSM-15606. The plasma stability evaluation over time showed lasting presence of >70% of parent compound at 30 min and close to 60% of parent compound at 60 min.

It was designed at the University of California, San Diego, synthesized at Albany Molecular Research, and determined to be >95% pure based on liquid chromatography–tandem mass spectrometry and nuclear magnetic resonance analyses. Mass spectrometry data were recorded on an Agilent 6310 ion trap mass spectrometer (electrospray ionization source) connected to an Agilent 1200 series HPLC with quaternary pump, vacuum degasser, diode-array detector, and autosampler. [¹¹C]CO$_2$ (1.0 Ci) was obtained via the 14N ($p$, $\alpha$)11C reaction on nitrogen with 2.5% oxygen, with 11 MeV protons (Siemens Eclipse cyclotron), and trapped on molecular sieves in a TRACERlab FX-MeI synthesizer (General Electric). [¹¹C]CH$_4$ was obtained by the reduction of [¹¹C]CO$_2$ in the presence of Ni/hydrogen at 350°C and recirculated through an oven containing I2 to produce 11CH3I via a radical reaction. All animal studies were performed at Massachusetts General Hospital (PHS Assurance of Compliance no. A3596-01). The Subcommittee on Research Animal Care serves as the Institutional Animal Care and Use Committee for the Massachusetts General Hospital. The Subcommittee on Research Animal Care reviewed and approved all procedures detailed in this paper.

**Synthesis of compound 1 (precursor)**
A mix of SGSM-15606 (10 mg, 0.024 mmol), NaI (11 mg, 0.073 mmol, 3 eq), and TMSCl (0.01 ml, 8.6 mg, 0.079 mmol, 3 eq) in MeCN (1.0 ml) was heated at 80°C for 2 h. The resulting mix was cooled to room temperature and subjected to silica gel chromatography to give the desired product as a brown solid (8 mg, 0.020 mmol, 84% yield; mass spectrometry electrospray ionization [M+H] + 405.2).

**Radiosynthesis of [¹¹C]SGSM-15606**
[¹¹C]CH3I was trapped in a TRACERlab FX-M synthesizer reactor (General Electric) preloaded with a solution of precursor (0.5 mg) Cs$_2$CO$_3$ (5.0 mg) in dry DMSO (300 µl). The solution was stirred at 50°C for 3 min, and water (1.2 ml) was added. The reaction mixture was purified by reverse phase semipreparative HPLC (Phenomenex Luna 5u C8(2), 250 mm × 10 mm, 5 µm, 5.0 ml/min, 50% H$_2$O + ammonium formate [0.1 M]/50% CH3CN), and the desired fraction was collected. The final product was reformulated by loading onto a solid-phase exchange C-18 cartridge, rinsing with water (5 ml) and eluting with EtOH (0.3 ml) and saline (0.9%, 2.7 ml). The chemical and radiochemical purity of the final product was tested by analytical HPLC (Agilent Eclipse XDB-C18, 150 mm × 4.6 mm). The average time required for the synthesis from end of cyclotron bombardment to end of synthesis was 35 min. The average radiochemical yield was 2–5% (nondecay corrected to trapped [¹¹C]CH3I). Chemical and radiochemical purities were ≥95% with a specific activity 0.8 ± 0.2 Ci/µmol (end of bombardment).

Xu et al.
Visualizing Alzheimer's gamma-secretase

**Journal of Experimental Medicine**    6 of 9
https://doi.org/10.1084/jem.20182266

## Rodent PET–computed tomography (CT) acquisition and postprocessing

Mice were used in this study. Animals were anesthetized with inhalational isoflurane (Forane) at 3% in a carrier of 1.5–2 liter/min medical oxygen and maintained at 2% isoflurane during the imaging scan. The mice were then arranged in a Triumph Tri-modality PET/CT/SPECT scanner (Gamma Medica) with a PET resolution of 1–1.5 mm. Radiolabeled compound (100–200 μCi per animal) was injected via lateral tail vein catheterization. For the blocking study, unlabeled compound was injected 5 min before the start of PET acquisition. Each dynamic PET scan was performed for 60 min and followed by CT.

## Rodent PET-CT image analysis

After scanning, dynamic PET data were collected and the corresponding images were reconstructed by 3D-MLEM (maximum likelihood expectation maximization) method. The spheres in brain regions were defined as the volumes of interest (VOIs) according to the high-resolution CT structural images and summed PET data, with a radius of no less than 1 mm to minimize partial volume effects. Reconstructed images were exported from the scanner in DICOM format along with an anatomical CT for rodent studies.

## Macaque PET-MR acquisition

One rhesus macaque (male, 13 yr old), deprived of food for 12 h before the study, was included in the PET-MRI scan. Anesthesia was induced with intramuscular xylazine (0.5–2.0 mg/kg) and ketamine (10 mg/kg). After endotracheal intubation, V-line and A-line were inserted, and anesthesia was maintained using isoflurane. The macaque was catheterized antecubitally for radiotracer injection, and a radial arterial line was placed for arterial blood sampling for blood and metabolite analysis. PET magnetic resonance images of the brain were acquired on a BrainPET insert on a Siemens TIM-Trio 3T MRI scanner with a PET resolution of ~2.5 mm at isocenter. Dynamic PET image acquisition was initiated followed by administration of 2 mCi [$^{11}$C]SGSM-15606. A multi-echo magnetization prepared rapid acquisition gradient echo (MEMPRAGE) sequence begin at the same time of the PET scan for anatomical coregistration. Dynamic data from the PET scan were recorded in list mode and corrected for attenuation. Macaque data were reconstructed using a 3D-OSEM (ordered subsets expectation-maximization) method.

## Macaques PET-MR image analysis

PET data were motion corrected, spatially smoothed with a 2.5-mm full-width at half-maximum Gaussian filter, and registered to the INIA19 Template and NeuroMaps Atlas for brain imaging analysis in macaques. Image registration was performed on high-resolution MPRAGE MRI image using a 12–degrees of freedom linear algorithm and a nonlinear algorithm to the atlas brain. The transformation was then applied to the simultaneously collected dynamic PET data. Kinetic modeling was performed in PMOD (PMOD3.4; PMOD Technologies). VOIs were selected according to the brain atlas. A common VOI mask was applied. TACs were exported from the whole brain and

brain regions for analysis. A 2-TC model was used to estimate regional $V_T$ (ml/cm$^3$) with a metabolite-corrected plasma TAC. Voxel-wise $V_T$ maps will be calculated using 2-TC from the dynamic PET data.

## Plasma and metabolite analysis

Arterial samples collected during imaging from the macaque were centrifuged to obtain plasma, which will be then removed and placed in an automated gamma counter. Metabolite analysis was conducted on a custom automated robot fitted with Phenomenex solid-phase exchange Strata-X 500 mg solid-phase extraction cartridges that will be primed with ethanol (2 ml) and deionized water (20 ml). Protein precipitation was achieved by addition of plasma (300 μl) to acetonitrile (300 μl), which was centrifuged for 1 min to obtain protein-free plasma. 300 μl protein-free plasma/acetonitrile solution was diluted into deionized water (3 ml), loaded onto the C18 cartridge, and removed of polar metabolites with 100% water. Next, a series of extractions were performed using water and acetonitrile. Each sample was counted in a WIZARD2 Automatic Gamma Counter to determine the presence of radiolabeled metabolites.

## Online supplemental material

Fig. S1 demonstrates the developmental stages of our GSMs. Table S1 lists the biochemical properties of SGSM-15606.

Author contributions: C. Wang and C. Zhang conceived the experiment. C. Wang, C. Zhang, R.E. Tanzi, D.R. Bernales, and R.E. Koegel performed experimental design and data interpretation. K.D. Rynearson and S.L. Wagner prepared SGSMs. Y. Xu, C. Wang, H.Y. Wey, Y. Liang, Z. Chen, C. Ran, S.H. Choi, K.D. Rynearson, D.R. Bernales, R.E. Koegel, S.A. Fiedler, and R. Striar

# References

Bai, X.C., C. Yan, G. Yang, P. Lu, D. Ma, L. Sun, R. Zhou, S.H.W. Scheres, and Y. Shi. 2015. An atomic structure of human γ-secretase. *Nature.* 525: 212–217. https://doi.org/10.1038/nature14892

Bertram, L., and R.E. Tanzi. 2008. Thirty years of Alzheimer's disease genetics: the implications of systematic meta-analyses. *Nat. Rev. Neurosci.* 9:768–778. https://doi.org/10.1038/nrn2494

Brendel, M., A. Jaworska, J. Herms, J. Trambauer, C. Rötzer, F.J. Gildehaus, J. Carlsen, P. Cumming, T. Luebbers, et al. 2015. Amyloid-PET predicts inhibition of de novo plaque formation upon chronic γ-secretase modulator treatment. *Mol. Psychiatry.* 20:1179–1187. https://doi.org/10.1038/mp.2015.74

Chávez-Gutiérrez, L., L. Bammens, I. Benilova, A. Vandersteen, M. Benurwar, M. Borgers, S. Lismont, L. Zhou, S. Van Cleynenbreugel, H. Esselmann, et al. 2012. The mechanism of γ-Secretase dysfunction in familial Alzheimer disease. *EMBO J.* 31:2261–2274. https://doi.org/10.1038/emboj.2012.79

Choe, Y.S., and K.H. Lee. 2015. PET Radioligands for Imaging of Tau Pathology: Current Status. *Nucl. Med. Mol. Imaging.* 49:251–257. https://doi.org/10.1007/s13139-015-0374-9

Choi, S.H., Y.H. Kim, M. Hebisch, C. Sliwinski, S. Lee, C. D'Avanzo, H. Chen, B. Hooli, C. Asselin, J. Muffat, et al. 2014. A three-dimensional human neural cell culture model of Alzheimer's disease. *Nature.* 515:274–278. https://doi.org/10.1038/nature13800

Cummings, J.L.. 2004. Alzheimer's disease. *N. Engl. J. Med.* 351:56–67. https://doi.org/10.1056/NEJMra040223

Gandy, S.. 2005. The role of cerebral amyloid beta accumulation in common forms of Alzheimer disease. *J. Clin. Invest.* 115:1121–1129.

Gertsik, N., D.M. Chau, and Y.M. Li. 2015. γ-Secretase Inhibitors and Modulators Induce Distinct Conformational Changes in the Active Sites of γ-Secretase and Signal Peptide Peptidase. *ACS Chem. Biol.* 10:1925–1931. https://doi.org/10.1021/acschembio.5b00321

Hardy, J., and D.J. Selkoe. 2002. The amyloid hypothesis of Alzheimer's disease: progress and problems on the road to therapeutics. *Science.* 297: 353–356. https://doi.org/10.1126/science.1072994

Iben, L.G., R.E. Olson, L.A. Balanda, S. Jayachandra, B.J. Robertson, V. Hay, J. Corradi, C.V. Prasad, R. Zaczek, C.F. Albright, et al. 2007. Signal peptide peptidase and gamma-secretase share equivalent inhibitor binding pharmacology. *J. Biol. Chem.* 282:36829–36836. https://doi.org/10.1074/jbc.M707002200

Imbimbo, B.P., E. Del Giudice, D. Colavito, A. D'Arrigo, M. Dalle Carbonare, G. Villetti, F. Facchinetti, R. Volta, V. Pietrini, M.F. Baroc, et al. 2007. 1-(3′,4′-Dichloro-2-fluoro[1,1′-biphenyl]-4-yl)-cyclopropanecarboxylic acid (CHF5074), a novel gamma-secretase modulator, reduces brain beta-amyloid pathology in a transgenic mouse model of Alzheimer's disease without causing peripheral toxicity. *J. Pharmacol. Exp. Ther.* 323: 822–830. https://doi.org/10.1124/jpet.107.129007

Imbimbo, B.P., E. Frigerio, M. Breda, F. Fiorentini, M. Fernandez, S. Sivilia, L. Giardino, L. Calzà, D. Norris, D. Casula, et al. 2013. Pharmacokinetics and pharmacodynamics of CHF5074 after short-term administration in healthy subjects. *Alzheimer Dis. Assoc. Disord.* 27:278–286. https://doi.org/10.1097/WAD.0b013e3182622ace

James, O.G., P.M. Doraiswamy, and S. Borges-Neto. 2015. PET Imaging of Tau Pathology in Alzheimer's Disease and Tauopathies. *Front. Neurol.* 6:38. https://doi.org/10.3389/fneur.2015.00038

Klunk, W.E., H. Engler, A. Nordberg, Y. Wang, G. Blomqvist, D.P. Holt, M. Bergström, I. Savitcheva, G.F. Huang, S. Estrada, et al. 2004. Imaging brain amyloid in Alzheimer's disease with Pittsburgh Compound-B. *Ann. Neurol.* 55:306–319. https://doi.org/10.1002/ana.20009

Kounnas, M.Z., A.M. Danks, S. Cheng, C. Tyree, E. Ackerman, X. Zhang, K. Ahn, P. Nguyen, D. Comer, L. Mao, et al. 2010. Modulation of gamma-secretase reduces beta-amyloid deposition in a transgenic mouse model of Alzheimer's disease. *Neuron.* 67:769–780. https://doi.org/10.1016/j.neuron.2010.08.018

Kreft, A.F., R. Martone, and A. Porte. 2009. Recent advances in the identification of gamma-secretase inhibitors to clinically test the Abeta oligomer hypothesis of Alzheimer's disease. *J. Med. Chem.* 52:6169–6188. https://doi.org/10.1021/jm900188z

Landau, S.M., B.A. Thomas, L. Thurfjell, M. Schmidt, R. Margolin, M. Mintun, M. Pontecorvo, S.L. Baker, and W.J. Jagust; Alzheimer's Disease Neuroimaging Initiative. 2014. Amyloid PET imaging in Alzheimer's disease: a comparison of three radiotracers. *Eur. J. Nucl. Med. Mol. Imaging.* 41:1398–1407. https://doi.org/10.1007/s00259-014-2753-3

Liu, F., Z.Q. Xue, S.H. Deng, X. Kun, X.G. Luo, P.R. Patrylo, G.M. Rose, H. Cai, R.G. Struble, Y. Cai, et al. 2013. γ-secretase binding sites in aged and Alzheimer's disease human cerebrum: the choroid plexus as a putative origin of CSF Aβ. *Eur. J. Neurosci.* 37:1714–1725. https://doi.org/10.1111/ejn.12159

Liu, L., L. Ding, M. Rovere, M.S. Wolfe, and D.J. Selkoe. 2019. A cellular complex of BACE1 and γ-secretase sequentially generates Aβ from its full-length precursor. *J. Cell Biol.* 218:644–663. https://doi.org/10.1083/jcb.201806205

Nordberg, A.. 2004. PET imaging of amyloid in Alzheimer's disease. *Lancet Neurol.* 3:519–527. https://doi.org/10.1016/S1474-4422(04)00853-1

Oakley, H., S.L. Cole, S. Logan, E. Maus, P. Shao, J. Craft, A. Guillozet-Bongaarts, M. Ohno, J. Disterhoft, L. Van Eldik, et al. 2006. Intraneuronal beta-amyloid aggregates, neurodegeneration, and neuron loss in transgenic mice with five familial Alzheimer's disease mutations: potential factors in amyloid plaque formation. *J. Neurosci.* 26:10129–10140. https://doi.org/10.1523/JNEUROSCI.1202-06.2006

Okamura, N., R. Harada, S. Furumoto, H. Arai, K. Yanai, and Y. Kudo. 2014. Tau PET imaging in Alzheimer's disease. *Curr. Neurol. Neurosci. Rep.* 14: 500. https://doi.org/10.1007/s11910-014-0500-6

Park, J., I. Wetzel, I. Marriott, D. Dréau, C. D'Avanzo, D.Y. Kim, R.E. Tanzi, and H. Cho. 2018. A 3D human triculture system modeling neurodegeneration and neuroinflammation in Alzheimer's disease. *Nat. Neurosci.* 21:941–951. https://doi.org/10.1038/s41593-018-0175-4

Patel, S., S. O'Malley, B. Connolly, W. Liu, R. Hargreaves, C. Sur, and R.E. Gibson. 2006. In vitro characterization of a gamma-secretase radiotracer in mammalian brain. *J. Neurochem.* 96:171–178. https://doi.org/10.1111/j.1471-4159.2005.03525.x

Pozdnyakov, N., H.E. Murrey, C.J. Crump, M. Pettersson, T.E. Ballard, C.W. Am Ende, K. Ahn, Y.M. Li, K.R. Bales, and D.S. Johnson. 2013. γ-Secretase modulator (GSM) photoaffinity probes reveal distinct allosteric binding sites on presenilin. *J. Biol. Chem.* 288:9710–9720. https://doi.org/10.1074/jbc.M112.398602

Raven, F., J.F. Ward, K.M. Zoltowska, Y. Wan, E. Bylykbashi, S.J. Miller, X. Shen, S.H. Choi, K.D. Rynearson, O. Berezovska, et al. 2017. Soluble Gamma-secretase Modulators Attenuate Alzheimer's β-amyloid Pathology and Induce Conformational Changes in Presenilin 1. *EBioMedicine.* 24:93–101. https://doi.org/10.1016/j.ebiom.2017.08.028

Rogers, K., K.M. Felsenstein, L. Hrdlicka, Z. Tu, F. Albayya, W. Lee, S. Hopp, M.J. Miller, D. Spaulding, Z. Yang, et al. 2012. Modulation of γ-secretase by EVP-0015962 reduces amyloid deposition and behavioral deficits in Tg2576 mice. *Mol. Neurodegener.* 7:61. https://doi.org/10.1186/1750-1326-7-61

Seo, Y.J., Y. Kang, L. Muench, A. Reid, S. Caesar, L. Jean, F. Wagner, E. Holson, S.J. Haggarty, P. Weiss, et al. 2014. Image-guided synthesis reveals potent blood-brain barrier permeable histone deacetylase inhibitors. *ACS Chem. Neurosci.* 5:588–596. https://doi.org/10.1021/cn500021p

Sivilia, S., L. Lorenzini, A. Giuliani, M. Gusciglio, M. Fernandez, V.A. Baldassarro, C. Mangano, L. Ferraro, V. Pietrini, M.F. Baroc, et al. 2013. Multi-target action of the novel anti-Alzheimer compound CHF5074: in vivo study of long term treatment in Tg2576 mice. *BMC Neurosci.* 14: 44. https://doi.org/10.1186/1471-2202-14-44

Wagner, S.L., C. Zhang, S. Cheng, P. Nguyen, X. Zhang, K.D. Rynearson, R. Wang, Y. Li, S.S. Sisodia, W.C. Mobley, et al. 2014. Soluble γ-secretase modulators selectively inhibit the production of the 42-amino acid amyloid β peptide variant and augment the production of multiple carboxy-truncated amyloid β species. *Biochemistry.* 53:702–713. https://doi.org/10.1021/bi401537v

Wagner, S.L., K.D. Rynearson, S.K. Duddy, C. Zhang, P.D. Nguyen, A. Becker, U. Vo, D. Masliah, L. Monte, J.B. Klee, et al. 2017. Pharmacological and Toxicological Properties of the Potent Oral γ-Secretase Modulator BPN-15606. *J. Pharmacol. Exp. Ther*. 362:31–44. https://doi.org/10.1124/jpet.117.240861

Wang, C., F.A. Schroeder, and J.M. Hooker. 2014. Visualizing epigenetics: current advances and advantages in HDAC PET imaging techniques. *Neuroscience*. 264:186–197. https://doi.org/10.1016/j.neuroscience.2013.09.018

Yan, X.X., T. Li, C.M. Rominger, S.R. Prakash, P.C. Wong, R.E. Olson, R. Zaczek, and Y.W. Li. 2004. Binding sites of gamma-secretase inhibitors in rodent brain: distribution, postnatal development, and effect of deafferentation. *J. Neurosci*. 24:2942–2952. https://doi.org/10.1523/JNEUROSCI.0092-04.2004

Youmans, K.L., L.M. Tai, T. Kanekiyo, W.B. Stine, Jr., S.C. Michon, E. Nwabuisi-Heath, A.M. Manelli, Y. Fu, S. Riordan, W.A. Eimer, et al. 2012. Intraneuronal Aβ detection in 5xFAD mice by a new Aβ-specific antibody. *Mol. Neurodegener*. 7:8. https://doi.org/10.1186/1750-1326-7-8

Zhang, C.. 2017. Developing effective therapeutics for Alzheimer's disease -- emerging mechanisms and actions in translational medicine. *Discov. Med*. 23:105–111.

Zhang, L., L. Chen, J.K. Dutra, E.M. Beck, S. Nag, A. Takano, N. Amini, R. Arakawa, M.A. Brodney, L.M. Buzon, et al. 2018. Identification of a Novel Positron Emission Tomography (PET) Ligand for Imaging β-Site Amyloid Precursor Protein Cleaving Enzyme 1 (BACE-1) in Brain. *J. Med. Chem*. 61:3296–3308. https://doi.org/10.1021/acs.jmedchem.7b01769

# Supplemental material
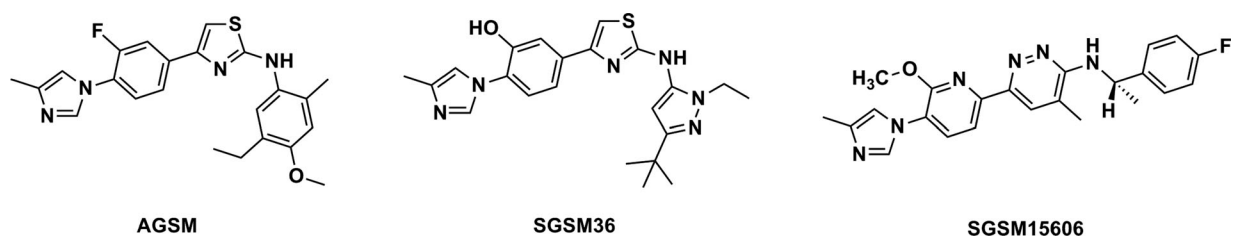


AGSM          SGSM36          SGSM15606

Figure S1.   **Development of our GSMs.** Our GSMs have been developed in three stages and displayed unique structures with different aqueous solubility and inhibitory effects on $A\beta_{42}$ levels (represented by $IC_{50}/A\beta_{42}$ values). Our parent GSM was an aryl 2-aminothiazole class GSM with relatively low aqueous solubility, which displayed low aqueous solubility ($IC_{50}/A\beta_{42}$ –10 nM). SGSM-36 was our first-generation soluble GSM and is an aryl 2-aminothiazole class compound ($IC_{50}/A\beta_{42}$ –100 nM). SGSM-15606 was our second-generation SGSM and was a highly potent pyridazine class SGSM ($IC_{50}/A\beta_{42}$ –7 nM).

**Table S1 is provided online and shows that SGSM-15606 displayed excellent properties for PET imaging probe development.**